The Pennsylvania State University

The Graduate School

Department of Aerospace Engineering

ANALYSIS OF CHEMISTRY MODELS FOR DSMC SIMULATIONS OF THE ATMOSPHERE OF IO

A Thesis in

Aerospace Engineering

by

Hao Deng

Submitted in Partial Fulfillment

of the Requirements

for the Degree of

Master of Science

May 2011

The thesis of Hao Deng was reviewed and approved* by the following:

Deborah A. Levin
Professor of Aerospace Engineering
Thesis Advisor

Michael M. Micci
Professor of Aerospace Engineering
Director of Graduate Studies

George A. Lesieutre
Professor of Aerospace Engineering
Head of Aerospace Engineering

*Signatures are on file in the Graduate School.

Abstract

Chemical reactions between sulfur dioxide and atomic oxygen are important in modeling the atmosphere of Io and since the atmosphere is sufficiently rarefied, the flow about the Jovian moon is usually modeled using DSMC. The chemical reaction rates between SO_2 and O obtained using the Molecular Dynamic/Quasi-Classical Trajectory (MD/QCT) method are compared with the Total Collisional Energy (TCE) model of Bird [1] and values in the literature. The implementation of both MD/QCT and TCE chemistry reaction models in DSMC is studied in a 0-D time dependent analysis and 2-D axisymmetric DSMC simulations. The MD/QCT simulations were found to result in lower reaction rate constants and reaction probabilities than the TCE model and the vibrational favoring feature of the $SO_2 + O \rightarrow SO + 2O$ reaction was revealed. A 2-D DSMC simulation of an approximate planetary flow consisting of a plume-counter flow between planetary outgassing sulfur dioxide and high energy free stream oxygen was performed. The flow conditions are such that the reference values used in obtaining the total VHS cross section are inadequate to describe the total collisional cross section. Therefore the total cross section using the more general viscosity cross section was obtained through the MD/QCT simulations and was found to have a significantly different energy dependence compared to the original VHS cross section. For the 2-D DSMC simulations it was found that the structure of the flow as well as the chemically formed sulfur oxide were different for the MD/QCT and the TCE reaction probabilities and total cross sections. In addition, the reaction region was found to be highly non-equilibrium, which suggests that MD/QCT is a more suitable chemistry model for the simulation of the Io's atmosphere.

Table of Contents

List of Figures

List of Tables

Acknowledgments

The research performed at the Pennsylvania State University was supported by the NASA through the grant No. NNX07AC47A. We would like to acknowledge Prof. M. Ivanov of the Institute of Theoretical and Applied Mechanics, Russia for the use of the original SMILE code. We also wish to acknowledge the useful conversations with Mr. Chris Moore and Profs. D. Goldstein and P. Varghese.

Chapter 1

Introduction

The nature of Io's atmosphere has attracted substantial scientific interest ever since the discovery of its ionosphere by the Pioneer spacecraft in 1973. [2] This active atmosphere, featuring distinctive volcanic plumes, has been studied for decades through observations by ground-based [3] and Earth-orbiting [4] telescopes and the targeted campaigns by the Galileo and Cassini missions as well as numerical modeling. [5, 6] Io's plumes are generated when volatile vapors are violently expelled from volcanoes, and evolve through processes including acceleration and cooling due to expansion and thermal radiation, forming a canopy shaped shock when the vent plume intersects with the descending flow, and finally depositing a ring of condensed material around the source region. [7] The series of gas dynamics processes occurring in the plumes and their effects on Io's surface and atmosphere are of great interest to the planetary atmosphere science community.

The direct simulation Monte Carlo (DSMC) method has been shown to be well suited to modeling the variety of plume dynamics and planetary phenomena occurring in the atmosphere of Io. These phenomena encompass a wide range of flow regimes where the continuum assumption breaks down and a kinetic rarefied gas model must be applied. An example of a planetary feature where this occurs is

the flow between the near vent flow and the much higher canopy shock. Extensive axisymmetric DSMC simulations were conducted by Austin and Goldstein [8, 9] and Zhang *et al* [7, 10, 11, 12], in which these and other physical phenomena were explored. Their work included hot band transition in the rotational radiation model, discrete line emission from the three SO_2 vibrational modes, coupled gas/dust flows, and multiple gas species. Although successfully explaining many aspects of the plume dynamics, they have not included chemical reactions in the simulations.

The relative composition of Io's atmosphere is not yet well known, but SO, O_2, S and O are expected to be created from SO_2 primarily by photo-dissociation and gas phase chemistry. In order to study this moon of Jupiter and its atmosphere, reactions between sulfur dioxide and atomic oxygen were initially investigated by Moghe [13], through Molecular Dynamic/Quasi-Classical Trajectories calculations. In that work, the three product paths which can be obtained from the dissociation process of SO_2 by collisional impact with atomic oxygen were considered,

$$SO_2 + O \rightarrow SO + O + O \tag{1.1}$$

$$SO_2 + O \rightarrow S + O + O_2 \tag{1.2}$$

$$SO_2 + O \rightarrow S + O + O + O \tag{1.3}$$

The first reaction was found to be the dominant mechanism for the conditions explored, and thus is the focus of this work.

Molecular Dynamic/Quasi-Classical (MD/QCT) simulations of a chemical reaction require the solution of Hamiltonian equations of motion for a specified initial reactant state followed with analyses of the obtained trajectory results. To perform molecular dynamics calculations, one has to know how the molecular system's electronic energy changes as a function of all inter-nuclear distances, quantified by

the potential energy surface (PES). The PES used in this work was a sum of Lennard-Jones 6-12 pairwise potentials. [13, 14] MD/QCT simulations of chemical reaction cross-sections pertinent to chemically reacting flows have been performed and used in both Navier-Stokes [15] and DSMC calculations of a hypersonic NO and water, [16, 17] respectively. In Sec. 2 we present the specific approach used in this work to obtain the total and reaction cross section for the chemical reaction given in Eq. 1.1.

The purpose of this paper is to offer a new, fundamental approach to examine the collisional dissociation of sulfur dioxide by beams of high velocity atomic oxygen, conditions relevant to Io's atmosphere, and to determine the sensitivity of the DSMC simulations to the use of fundamentally obtained MD/QCT reaction probabilities and viscosity cross sections compared to the conventionally used TCE model and the VHS model based on Bird's values. [1] In Sec. 3, the chemical rate constants obtained by the integration of the MD/QCT reaction cross sections are compared with those estimated from the work of Moses *et al* [5] and Grillo *et al* [18]. The latter chemical rates are used in the planetary atmospheric modeling of Io, but their use is problematic because they were derived from very different conditions. In the following section, we investigate different approaches for incorporating the MD/QCT reaction cross sections into DSMC simulations and compare the outcomes of two different approaches with the results obtained using the original TCE model based on the experiments of Grillo.[18] The sensitivity of the chemistry models is explored in 0-D DSMC simulations which are validated by comparison with simple, semi-analytic numerical integration of a chemical rate equation. The differences between the TCE model and the MD/QCT approach, in terms of vibrational favoring, is discussed. Next in Sec. 5, the limit of the reaction probabilities whether they are based on either the TCE or the MD/QCT reaction

cross sections is discussed and motivates the use of the MD/QCT viscosity cross section as a more realistic replacement to the VHS model that is based on the low temperature parameters given by Bird.[1] In that section, the MD/QCT viscosity cross sections and new reaction probabilities are obtained and are shown to provide more physically meaningful reaction probabilities, particularly at the very high relative collision velocities that will be relevant to the modeling of Io's atmosphere. Finally, in Sec. 6 we present 2-D axisymmetric DSMC simulations performed to evaluate the sensitivity of a plume-counterflow problem to the MD/QCT based collision model and chemistry models. The plume-counter flow problem represents a simplified, but important element of the planetary gas dynamics of Io.

Chapter 2

Description of the MD/QCT Approach

The MD/QCT calculations are the solutions of Hamilton's equations,

$$\dot{p}_{i,j} = -\frac{\partial V}{\partial r_{i,j}} \quad \text{and} \quad \dot{r}_{i,j} = -\frac{p_{i,j}}{m_i} \tag{2.1}$$

where the dotted symbol denotes a time derivative, V represents the total potential for the system of n atoms, $p_{i,j}$ and $r_{i,j}$ are the Cartesian momenta and coordinates for the i-th atom in the j-th direction, and m_i is the mass of the i-th atom. These coupled equations can be solved for the coordinates and momenta of the n-atom system using a fourth order Runge-Kutta method. [19] The integration is performed for a fixed length of time or until a specified condition is met, *e.g.,* the dissociation of the target molecule occurs, and the final states of each atom, *i.e.,* the coordinates and momenta, are recorded for further analysis.

A PES has been developed for the modeling of SO_2+O collisions [13, 14] which assumes that SO_2 molecule has a potential of the central force field type. [20] For

the collision pair system, the total potential is separated into

$$V(q_1, ..., q_{12}) = V_{mol} + V_{int} \tag{2.2}$$

where $q_1, ..., q_{12}$ denote the coordinates of the atoms of SO_2 and O, V_{mol} is the SO_2 molecular potential, and V_{int} is the collisional interaction potential between SO_2 and O. In this work, V_{mol} were modeled by using three Morse bond potentials as follows.

$$V_{mol} = \phi_{12}(r_{12}) + \phi_{13}(r_{13}) + \phi_{23}(r_{23}) \tag{2.3}$$

where $\phi_{ij}(r_{ij})$ is the pair potential between atoms i and j with a separation of r_{ij}. The parameters for this representation are given in the Table 2.1. [21] The Morse parameters were chosen so that the dissociation energy, the equilibrium bond lengths, and the bond angle of the isolated molecules can be reproduced. The normal mode frequencies in Table 2.1 were obtained from power spectra of low energy trajectories of an isolated SO_2 molecule with harmonic pair potentials.

The collisional interaction was modeled by pair interactions of the form

$$V_{int} = \phi_{14}(r_{14}) + \phi_{24}(r_{24}) + \phi_{34}(r_{34}) \tag{2.4}$$

as suggested by the work of Redmon *et al.* [22] The pair interactions are computed by using the standard Lennard-Jones 6-12 pair potentials as follows.

$$\phi_{ij}(r_{ij}) = 4\epsilon_{ij}\left[\left(\frac{\sigma_{ij}}{r_{ij}}\right)^{12} - \left(\frac{\sigma_{ij}}{r_{ij}}\right)^{6}\right] \tag{2.5}$$

and as an approximation, all Lennard-Jones parameters for the atom-centered pair interactions were taken to be identical and were obtained by using the combining

rules,

$$\sigma_{SO_2-O} = \frac{1}{2}(\sigma_{SO_2} + \sigma_O) = 3.668\ \dot{A}^2 \tag{2.6}$$

$$\epsilon_{SO_2-O} = \sqrt{(\epsilon_{SO_2}\epsilon_O)} = 173.68\ \text{K} \tag{2.7}$$

In order to perform MD/QCT calculations, the initial conditions of the collision pair, *i.e.,* the collider O and each atom of the target SO_2, have to be specified. The specification of the initial conditions depends on the problem to be solved. For the use of the MD/QCT results in a DSMC simulation, this is usually done by sampling the initial conditions of the target molecule with the same internal energy at a fixed the relative collisional velocity for the collider. Microcanonical sampling [17] was employed in this work to generate the initial conditions for the target molecule, in which the coordinates and momenta are determined separately. Further details regarding the implementation of the microcanonical sampling and the preparation of the DSMC reaction data base may be found in Ref. [14].

Table 2.1. Parameters for the SO_2 potential energy surface.[a]

SO equilibrium distance in SO_2	r^e_{12},r^e_{13}	1.4321 Å
O-O equilibrium distance in SO_2	r^e_{23}	2.4742 Å
O-S-O equilibrium bond angle	θ^e_{O-S-O}	119.5°
Morse range parameters	β_{12},β_{13},β_{23}	2.4 $Å^{-1}$
Morse dissociation energies	D_{12}=D_{13}=D_{SO}	100 kcal/mole
Morse dissociation energy	D_{23}	30.5 kcal/mole
dissociation energy	D_{SO-O}=D_{SO}+D_{OO}	130.5 kcal/mole
vibration frequency	asymmetric stretch	1213 cm^{-1}
vibration frequency	symmetric stretch	1187 cm^{-1}
vibration frequency	bend	394 cm^{-1}

[a] The Morse potential is defined as $\phi_{ij}(r_{ij}) = D_{ij}\left[1 - \exp\left\{-\beta_{ij}(r_{ij} - r^e_{ij})\right\}\right]^2$ where r^e_{ij} is the equilibrium internuclear distance.

Chapter 3

Rate Constants Derived from MD/QCT Results

Although, the MD/QCT reaction cross-section, σ_R, is the fundamental physical quantity in modeling collisions that result in chemical reactions, most often it cannot be directly compared with experimental data. Generally the chemical reaction rate, rather than the cross-section is available, and for this reason, we consider the latter by using the following kinetic relationship for the rate in terms of the reaction cross-section,

$$k_d(T) = \int_0^\infty \int_0^\infty v_r f(v_r) f(E_{int}) \sigma_R(E_{int}, v_r) dE_{int} dv_r \tag{3.1}$$

where

$$f(E_{int}) = \frac{E_{int}^{\zeta_{int}/2-1}}{\Gamma(\zeta_{int}/2)(kT)^{\zeta_{int}/2}} \exp\left(-\frac{E_{int}}{kT}\right) \tag{3.2}$$

and

$$f(v_r) = \frac{4m_r^{3/2} v_r^2}{\pi^{1/2}(2kT)^{3/2}} \exp\left(-\frac{m_r v_r^2}{2kT}\right) \tag{3.3}$$

In the above equations, $k_d(T)$ is the dissociation reaction rate, $f(E_{int})$ is the distribution function for internal energy, $f(v_r)$ is the distribution function for relative velocity, σ_R is the reaction cross-section, ζ_{int} is the number of internal degrees of freedom, and m_r is the reduced mass of SO_2 and O. Since the internal energy, E_{int}, can not be higher than the dissociation energy, the dissociation energy of SO_2, $E_{dis} = 9.07 \times 10^{-19}$ J was taken to be the upper limit of the internal energy in the MD/QCT calculations.

Figure 3.1 presents a comparison of the rate constants obtained from the MD/QCT calculations computed for several SO_2 internal energies over a range of $0.5{\times}10^{-19}$ to $9.0{\times}10^{-19}$ J with the work of Moses [5], Grillo [18], Astholz [23], and Olschewski [24]. In the work of Moses, the rate constant was given for the process $SO{+}O_2 \rightarrow SO_2{+}O$, the reverse process of interest and only at temperatures of 230-420 K. The rate shown in Fig. 3.1, designated as "Derivation from Moses", was obtained assuming detailed balance and the use of thermodynamic chemistry databases. [25, 26] Among the experimental results of Grillo, Astholz and Olschewski, Grillo's is the most recent. The experiments of Grillo [18] provide the rate constant for $SO_2{+}M{\rightarrow}SO{+}O{+}M$, however, only in the temperature range from 2500 to 5200 K, with M representing a third chemical species, such as, O, in our case. The Arrhenius parameters used in our paper are summarized in Table 3.1. In Fig. 3.1, the MD/QCT integrations were performed over the entire temperature range, whereas, the rate constants derived from the other two sources [5, 18, 23, 24] were only for low temperatures. The rate of Grillo [18] has been extended to higher temperatures (indicated by the enclosed square symbols) without justification. Note that a search of the literature did not reveal rates at temperatures higher than 7700 K. As shown in Fig. 3.1, the rate constant from the MD/QCT calculations falls between those of Grillo, Astholz and Olschewski,

and is closer to these three sources than the result of Moses. The MD/QCT results predict a rate constant lower in magnitude than that of Grillo throughout the temperature range, but both have similar temperature dependence. In terms of the Arrhenius parameters, the pre-exponential factor, Λ, from the MD/QCT calculations is approximately one order of magnitude lower than that of Grillo but the activation energy, E_a, is close.

Table 3.1. Summary of Arrhenius Parameters.[a]

Reaction	Λ ($m^3s^{-1}mol^{-1}$)	η	E_a ($\times 10^{20}$J)	Temperature (K)	Source
$SO+O_2 \rightarrow SO_2+O$	2.6×10^{-19}	0	3.314	230-420	[b]
$SO_2+O \rightarrow SO+O_2$	2.985×10^{-22}	0.8484	5.619	3,000-10,000	[c]
$SO_2+O \rightarrow SO+O_2$	4.42×10^{-27}	3.02	124.3	10000-14000	[d]
$SO_2+O \rightarrow SO+2O$	2.491×10^{-14}	0	77.82	2,500-5,200	[e]
$SO_2+O \rightarrow SO+2O$	7.729×10^{-15}	0.25	90.00	3,000-14,000	[f]

[a] Λ is the pre-exponential factor, η is the temperature dependence, and E_a is the activation energy of the standard Arrhenius form, $k_d(T) = \Lambda T^{\eta} \exp(-E_a/kT)$.
[b] Moses [5]
[c] Derived [5, 25, 26]
[d] Derived [5, 25, 26]
[e] Grillo [18]
[f] Curve-fits of the MD/QCT reaction cross-section.

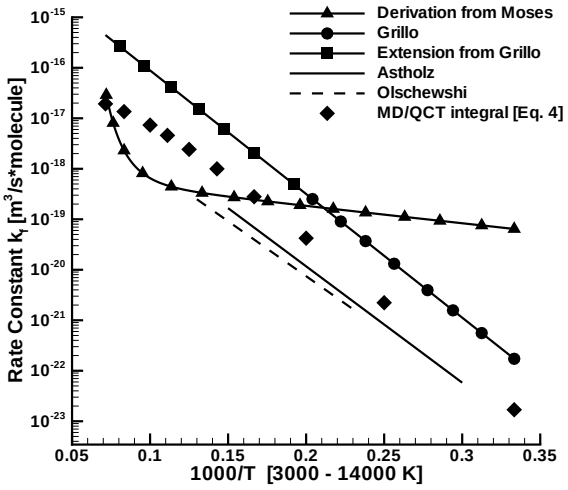

Figure 3.1. Comparison of reaction rate constants obtained from the literature and the new MD/QCT approach.

Chapter 4

Implementation of MD/QCT Reaction Cross Section in 0-D DSMC Simulations

4.1 Validation of 0-D DSMC Simulations

To validate our implementation of the MD/QCT derived chemistry model in DSMC we considered first a homogeneous gas or 0-D, time dependent DSMC simulation. To model chemical reactions in DSMC, reaction probabilities rather than rate constants are directly utilized and the traditional method for calculating the reaction probability is the TCE model of Bird. [1] In this model, the reaction probability has a special form that allows one to reproduce the experimental reaction rate $k_d(T)$ given in the standard Arrhenius form. Although the temperature, corresponding to the total collisional energy of interest, is high and exceeds the applicable range of the rate constants of both Moses [5] and Grillo [18], we use the Arrhenius parameters of Grillo in the TCE model, because their rates, as mentioned above, cover a higher temperature range than those of Moses [5] and are more recent than those

of Astholz [23] and Olschewski [24]. The DSMC simulations are then compared with semi-analytic results that are obtained through the numerical integration of the chemical rate kinetic equation

$$\frac{dn_{\mathrm{SO_2}}}{dt} = -n_{\mathrm{SO_2}} n_{\mathrm{O}} k_d \tag{4.1}$$

where $n_{\mathrm{SO_2}}$ and n_{O} are the time dependent chemical species number densities, and k_d is the dissociation reaction rate constant. To evaluate the dissociation rate coefficient, $k_d(T)$, the instantaneous temperature must be known. It is evaluated at each time step in the simulation as,

$$T' = \frac{(\zeta_{tot}^{\mathrm{SO_2}} n_{\mathrm{SO_2}} + \zeta_{tot}^{\mathrm{SO}} n_{\mathrm{SO}} + \zeta_{tot}^{\mathrm{O}} n_{\mathrm{O}} + \zeta_{tot}^{\mathrm{O}} n_{\mathrm{O}} - (n_{\mathrm{SO_2}} - n'_{\mathrm{SO_2}}) H_r/k) T}{\zeta_{tot}^{\mathrm{SO_2}} n'_{\mathrm{SO_2}} + \zeta_{tot}^{\mathrm{SO}} n'_{\mathrm{SO}} + \zeta_{tot}^{\mathrm{O}} n'_{\mathrm{O}} + \zeta_{tot}^{\mathrm{O}} n'_{\mathrm{O}}} \tag{4.2}$$

where H_r is the reaction heat, and the variables with and without prime represent the number densities at the end and the beginning of a time step, respectively.

The 0-D, time dependent DSMC calculation of a chemical reaction is performed in the SMILE/DSMC tool [27] as follows. The Majorant Frequency Scheme of Ivanov [28] is used to select particles for collision using the variable hard sphere (VHS) total cross-section model. [1] The Larsen-Borgnakke model [29] is used to re-distribute the translational and internal energies of the collision pair. The Millikan and White's collision number [30] is used for the vibration-translation relaxation, and Parker's collision number [31] is used for the rotation-translation relaxation. The reaction probability is then evaluated using the following expression of the TCE model:

$$P(E_c) = \frac{\pi^{1/2}\varepsilon\Lambda T_{ref}^{\eta}}{2\sigma_{ref}(kT_{ref})^{\eta-1+\omega_{\mathrm{AB}}}} \frac{\Gamma(\overline{\zeta}_{int}+5/2-\omega_{\mathrm{AB}})}{\Gamma(\overline{\zeta}_{int}+\eta+3/2)} \left(\frac{m_r}{2kT_{ref}}\right)^{1/2} \frac{(E_c-E_a)^{\eta+\overline{\zeta}_{int}+1/2}}{E_c^{\overline{\zeta}_{int}+3/2-\omega_{\mathrm{AB}}}} \tag{4.3}$$

where E_c is the total collisional energy, $\epsilon = 1$ is the symmetry factor, $\overline{\zeta}_{int}$ is the mean number of internal degrees of freedom, σ_{ref} is the total cross-section at the reference temperature T_{ref}, and ω_{AB} is the mean viscosity index of the reactants $SO_2 + O$.

Note that the viscosity index, ω, of the variable hard sphere model [1] was used and the rotational and vibrational degrees of freedom for SO_2 and SO were fixed to be the maximum possible value given by a simple harmonic oscillator model ($\zeta_{rot}^{SO_2} = 3$, $\zeta_{vib}^{SO_2} = 6$, $\zeta_{rot}^{SO} = 2$, $\zeta_{vib}^{SO} = 2$). This simplification in the DSMC simulation is not required in practice, but provides a better correspondence to the ideal equilibrium condition implied by the analytical solution, Eq. 4.1. The Arrhenius parameters of Grillo were used in both the TCE model to calculate the reaction probability for DSMC and the direct numerical integration of Eq. 4.1. Based upon the derivation of TCE model [1], the results from the 0-D DSMC simulation with the TCE model and the analytical solution should be the same.

Figure 4.1 shows the number densities of atomic oxygen from the 0-D DSMC simulations for gas temperatures of 15,000 and 6,000 K as a function of reaction time. The computational domain consisted of two, 2 (cm) by 2 (cm) cells and the wall boundary conditions were specular. The numerical parameters used to perform time dependent simulation of the two chemical species number density evolution are summarized in Table 4.1. The time dependent chemical concentrations were sampled over approximately 8,000 and 7,500 collisions per time step. Note that species weighting factors were not employed. The simulations start with the reactants of SO_2 and O in the system at the same concentration,

3.0×10^{22} molecule/m^3. As the dissociation reaction develops, the number density of SO_2 decreases and the concentrations of the products O and SO increase. In addition, the gas temperature decreases by about 35% because the chemical reaction of SO_2 + O is endothermic.

Examination of Fig. 4.1 shows that the chemical species number density, as a function of time, predicted by the DSMC/TCE model is close to that of the analytic solution for the higher temperature case, however, small discrepancies between the two may be observed, particularly for the lower temperature case. The reason for this discrepancy lies in the equilibrium assumption of the TCE model and its use in DSMC. The derivation of the TCE reaction probability assumes that the reactants exist in an equilibrium Maxwell-Boltzmann (MB) distribution at the total collisional energy, E_c, as shown in Fig. 4.2, at temperatures of 15,000 and 6,000 K. When determining if two particles will react, the total collisional energy must be greater than the activation energy, $E_a = 7.782 \times 10^{-19}$ J (shown as the cutoff line on the figure). Therefore, at a temperature of 15,000 K approximately one third of the area under the energy distribution curve (or one third of the numerical collisions) is eliminated. As the dissociation reaction proceeds, the chemical system keeps losing the SO_2 particles from the high energy portion of the distribution and there is insufficient time for the newly generated particles to relax with the rest of the system to a state of a MB equilibrium distribution. As shown in Fig. 4.1, for the lower temperature of 6,000 K the discrepancy between the TCE/DSMC and the analytic result is even larger, consistent with the fact that the majority of particles at the lower temperature have a total collisional energy less than the activation energy (see Fig. 4.2).

4.2 Further Investigation of the MD/QCT Model Implementation in DSMC Simulations

As mentioned above, the reaction probability is the parameter used directly in the DSMC modeling of chemical reactions. In this section, we will examine two approaches that can be used to derive reaction probabilities from the MD/QCT results and then examine the implementation of these different methods by testing them in 0-D DSMC simulations.

The first method, the more accurate approach, is to tabulate a number of reaction probabilities and then interpolate in the DSMC simulations as needed. In the MD/QCT calculation [13, 14], the reaction cross-section σ_R, is computed as a function of internal energy E_{int} and relative translational energy E_{tr}. By fixing E_{int} and varying E_{tr}, the MD/QCT reaction cross-sections as a function of the total collisional energy, defined by $E_c = E_{int} + E_{tr}$, are obtained. In addition, the total collisional cross-section σ_T^{VHS} is calculated using [1]

$$\sigma_T^{VHS} = \sigma_{ref} \left[\left\{ 2kT_{ref}/(m_r v_r^2) \right\}^{\omega_{\mathrm{AB}}-1/2} / \Gamma(5/2 - \omega_{\mathrm{AB}}) \right] \tag{4.4}$$

Reaction cross-sections as a function of collisional energy are shown in Fig. 4.3 (LHS) for five series of internal energy values, i.e., $E_{int} = 0.5 \times 10^{-19}, 2.0 \times 10^{-19}, 4.0 \times 10^{-19}, 6.0 \times 10^{-19}$, and 9.0×10^{-19} J. Using values such as these, the MD/QCT reaction probability P, the ratio of the reaction to the variable hard sphere cross-section, σ_R/σ_T^{VHS}, was calculated. Figure 4.3(RHS) shows the comparison of reaction probability between the MD/QCT calculations (enclosed symbols) and the TCE model using the Arrhenius parameters obtained by fitting to the data of Grillo [18] (open triangles). The location along the abscissa where the reaction probability starts to increase rapidly from zero is related to the acti-

vation energy for each case. We can see that the activation energy predicted by the MD/QCT calculations is close to that obtained from the rate constant fit of Grillo's data. Curves of both methods show that reaction probability increases with total collisional energy, and the reaction probabilities predicted by the TCE model are bounded by those from the MD/QCT calculations. Figure 4.3(RHS) also shows that, based upon the MD/QCT calculations, there is an indication of vibrational (or internal) favoring for the SO_2+O reaction [32, 16, 17]. For example, consider the points A and B on the curve for $E_{int} = 0.5 \times 10^{-19}$ J, and C on the curve for $E_{int} = 4.0 \times 10^{-19}$ J. The change of reaction probability is approximately 0.4, for point A compared to point B and corresponds to a change in the collisional energy, ΔE_c, which in this case is the same as the change in translational energy of approximately 3.5×10^{-19} J. A second comparison in the change of reaction probability for point A compared to point C is approximately 0.6. In that case, the change in ΔE_c between the A and C condition is the same as the change in internal energy and is also equal to 3.5×10^{-19} J. Therefore, for the same value of ΔE_c, the increase in reaction probability resulting from an increase of internal energy is greater than that from the increase of relative translational energy, an indication of vibrational favoring.

In the TCE model, the reaction cross-section is obtained through the following relationship

$$\sigma_R = \sigma_T^{VHS} C_1 (E_c - E_a)^{C_2} \left(1 - \frac{E_a}{E_c}\right)^{\overline{\zeta}_{int}+3/2-\omega_{\mathrm{AB}}} \tag{4.5}$$

and the constants C_1 and C_2 are calculated as,

$$C_1 = \frac{\pi^{1/2}\epsilon\Lambda T_{ref}^{\eta}}{2\sigma_{ref}} \frac{\Gamma(\overline{\zeta}_{int} + 5/2 - \omega_{\mathrm{AB}})}{\Gamma(\overline{\zeta}_{int} + \eta + 3/2)} \left(\frac{m_r}{2kT_{ref}}\right)^{1/2} \frac{T_{ref}^{1-\omega_{\mathrm{AB}}}}{k^{\eta-1+\omega_{\mathrm{AB}}}} \tag{4.6}$$

$$C_2 = \eta - 1 + \omega_{\mathrm{AB}} \tag{4.7}$$

Therefore, we propose a second method to implement the MD/QCT results in DSMC, in which the MD/QCT-derived reaction cross-sections are fit directly to Eq. 4.5 to obtain the constants C_1 and C_2. The Arrhenius parameters are then derived from these two constants, thus leading back to the reaction probability through the TCE model. Since the reaction cross-section in Eq. 4.5 is a function of the total collisional energy and the total cross-section in Eq. 4.4 is a function of the relative collisional velocity v_r, the analysis was simplified by choosing a fixed internal energy of $E_{int} = 4.0 \times 10^{-19}$. The Arrhenius parameters obtained from the fit are given in the last row of Table 3.1. Figure 4.3(LHS) shows the cross-section obtained from fitting the MD/QCT results in this manner and is designated as "σ_r fitting". It can be seen that the curve-fitted result is close to the MD/QCT calculated reaction cross-section curves, indicated by the enclosed symbols and lies midway between the highest and lowest internal energy value, consistent with the fixed internal energy chosen. The resulting reaction probability shown in Fig. 4.3(RHS) is close to the corresponding MD/QCT look-up table case.

Having obtained the reaction probabilities for these two approaches, 0-D DSMC simulations were performed for both methods using the VHS collision parameters and temperature dependent internal degrees of freedom. The cases were set up in the same way as described in Sec. 4.1, except that, the translational and internal temperatures were both initialized according to the specified translational and internal energies. Figure 4.4 shows a comparison between the two methods that use the MD/QCT reaction cross sections in a 0-D DSMC calculation. The initial condition of this case corresponds to a total collisional energy $E_c = 1.8 \times 10^{-18}$ J and an internal energy for the sulfur dioxide of $E_{int} = 9.0 \times 10^{-19}$ J, a value just below the dissociation limit of the molecule. Consistent with the reaction probabilities shown in Fig. 4.3 (RHS), the reactant number densities are close to each

other for the direct MD/QCT tabular method and the σ_R curve-fitting method. This suggests that use of the σ_R curve-fitting method to implement the MD/QCT reaction cross section in a TCE-like format gives a good approximation to the direct tabulation of the MD/QCT reaction probabilities in a DSMC simulation.

Furthermore, in order to examine the sensitivity to the ratio of the internal energy to the total collisional energy, two more sets of 0-D DSMC simulations were performed using these two methods. The initial internal energy was reduced to $E_{int} = 1.6 \times 10^{-20}$ J while the total collisional energy was kept the same as in Fig. 4.4. As shown in Fig. 4.5(LHS), the first method leads to slower reactions as the internal energy is reduced, which demonstrates again the vibrational favoring feature from the tabulated MD/QCT reaction probabilities. A similar change may be observed in Fig. 4.5(RHS) for the second method. However, this is not directly due to vibrational favoring, but rather occurs because although the TCE model assumes an equilibrium condition, the reaction probability is not only determined by the total collisional energy, but also by the number of internal degrees of freedom, ζ_{int}, which further depends on the gas temperature. Therefore, according to the TCE model, as the gas temperature decreases due to the lower initial E_{int}, the reaction also slows down.

A recent work by Ozawa *et al.* [32] demonstrated the importance of MD/QCT calculations to obtain both reaction and collision cross-sections for use in a DSMC simulation of hypervelocity collisional impact. In their work, good agreement between the TCE and MD/QCT model was observed for the O + HCl exchange reaction because the reaction does not show strong vibrational favoring. In this work, O + SO_2 reaction presents vibrational favoring effect, and thus, for applications under nonequilibrium conditions, the MD/QCT chemistry model is more preferable than the TCE model.

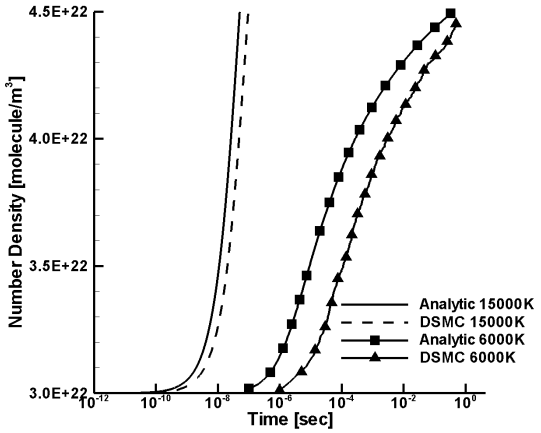

Figure 4.1. Time dependent number densities of atomic oxygen in the chemical reaction of $SO_2 + O \rightarrow SO + 2O$ in 0-D DSMC simulations for initial temperature of 15000 K and 6000 K.

Table 4.1. 0-D DSMC Simulation Numerical Parameters

Case	Temperature (K)	Time step (s)	Collisions sampled per step
1	6,000	10^{-6}	7,500
2	15,000	10^{-10}	8,000

Viscosity index ω [1] for species O and SO_2 used was 0.75 and 1.05, respectively.

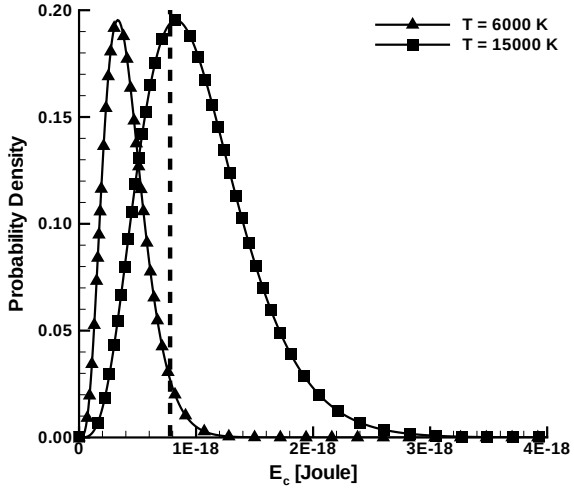

Figure 4.2. Maxwell-Boltzmann distributions at temperature of $6,000$ K and $1,5000$ K. The dashed vertical line indicates a cutoff of the total collisional energy E_c, which is equal to the activation energy, $E_a = 7.782 \times 10^{-19}$ J.

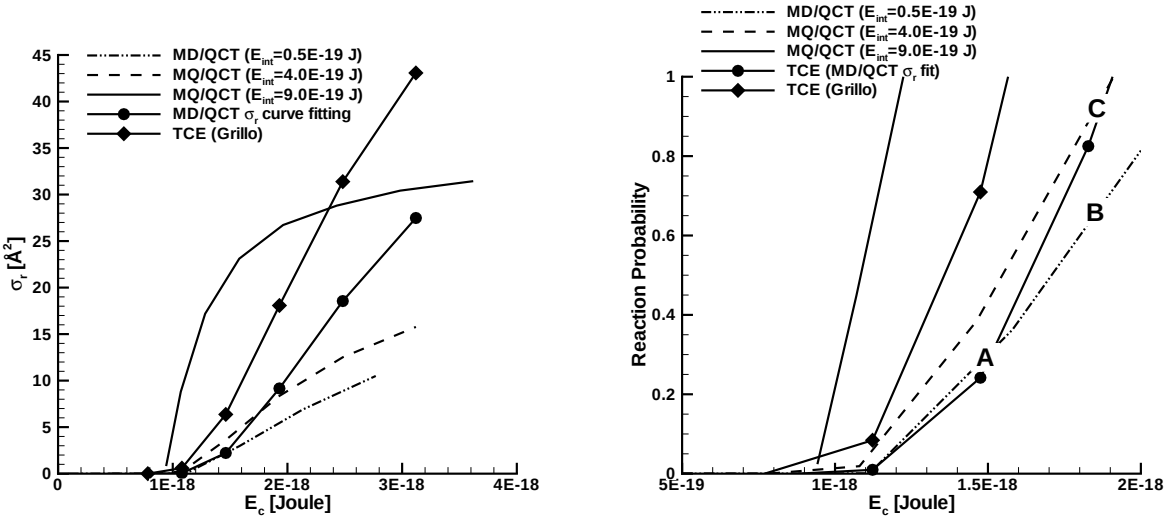

Figure 4.3. Comparison of reaction cross-sections (LHS) and reaction probability (RHS) as a function of total collisional energy for different models. Note that points A and B correspond to the $E_{int} = 0.5 \times 10^{-19}$ J curve and point C is on the $E_{int} = 4.0 \times 10^{-19}$ J curve.

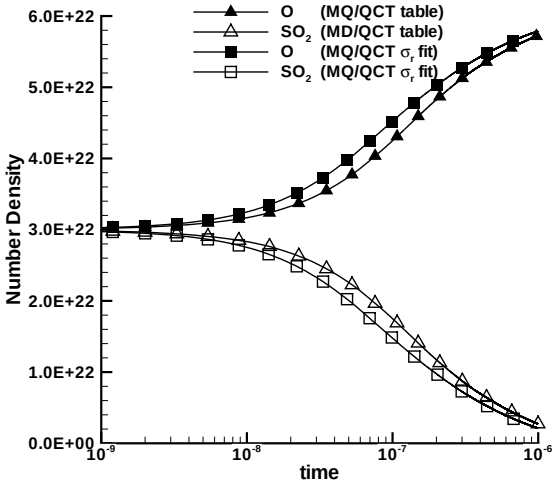

Figure 4.4. 0-D DSMC simulations: MD/QCT table, TCE using MD result integral curve-fitting, and TCE using σ_R curve-fitting, with $E_c = 1.8 \times 10^{-18}$ J and $E_{int} = 9.0 \times 10^{-19}$ J as the initial conditions.

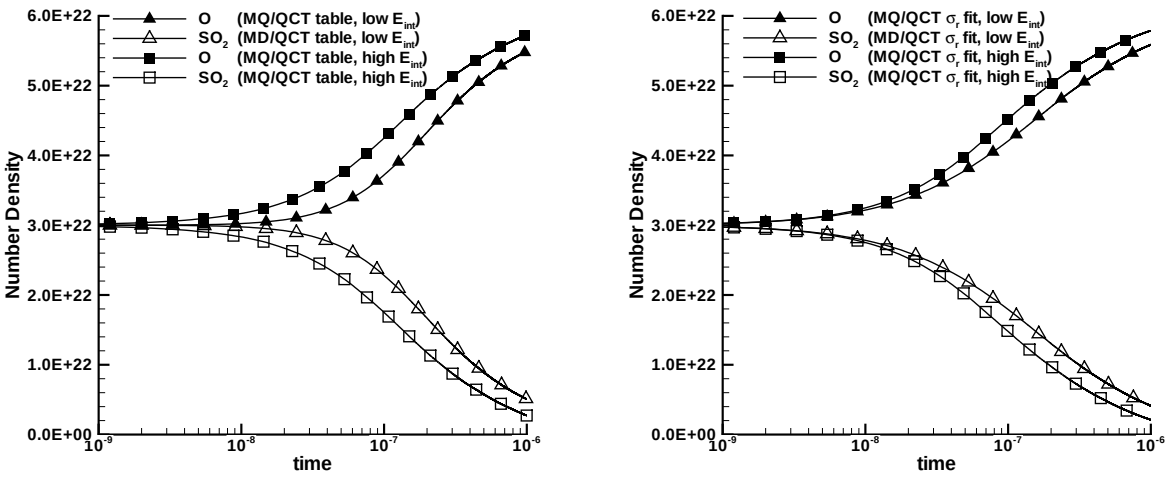

Figure 4.5. Sensitivity to E_{int}: (LHS) MD table vs. (RHS) TCE using σ_R curve-fitting. In both cases, the high and low value of E_{int} was set to be 9.0×10^{-19} and 1.6×10^{-20} J respectively, while E_c was kept to be the same as 1.8×10^{-18} J for the initial condition.

Chapter 5

MD/QCT Viscosity Cross Sections Based VHS Model for DSMC

Regardless of how the reaction cross section is obtained, *i.e,* using the TCE model or MD/QCT, the reaction probability must be less than unity. As indicated by Fig. 4.3 (RHS), that limit will be reached at different collision energy values for different models at high relative collisional energy impacts. For the conditions of Io, this poses a significant challenge in the DSMC simulation because there is the possibility of selecting particles with relative velocities that would result in an unphysical reaction probability being greater than one. Therefore in these simulations we need to check that this does not occur, and in particular, we need to check that there is no significant amount of collisions between O and SO_2 that exceed the collision energy limit.

Since our ultimate goal is to understand the sensitivity of the Io planetary gas dynamics to the hypervelocity chemistry model, we modeled a source of sulfur dioxide out gassing at a speed of 10 km/s from a sphere (*e.g.,* a planet) into a

constant opposing flow of atomic oxygen of 10 km/s. We will discuss the physics of these simulations in much more detail in Sec. 6. During the DSMC simulation we evaluated the locations in the flow where the reaction probability, based on the ratio of the TCE reaction cross section to the VHS total cross section, was found to be greater than unity. Figure 5.1 shows that there are areas very close to the sphere where this could occur and therefore suggests the need to obtain better total cross sections than the baseline-VHS model so that the applicability of the chemistry models can be extended to higher collision velocities. In the actual DSMC simulation, the reaction probability would be artificially cut off at unity and one would over count the actual number of reactions. An examination of the relative velocities at the points shown in Fig. 5.1 shows that they are consistent with the limit of the TCE reaction probability cut off for the curve labeled "TCE-Grillo" shown in Fig. 4.3.

Typically the DSMC method uses the conventional VHS model, but, it is not clear that our potential function will give a viscosity based total cross section that corresponds to that of a variable hard sphere using the usual low-temperature reference parameters. We could attempt to calculate the total cross section directly from our PES but the unboundedness of the classical total cross section will most likely make our result ambiguous as we would attempt to choose a maximum cut-off deflection angle. Therefore, as in our past work, we have found the approach of Tokumasu and Matsumoto[33] to be helpful in obtaining a viscosity-based cross section based on our specific PES. The equivalent VHS collision cross section, $\sigma_{VHS,MD}$, can be obtained based on the viscosity cross section, $\sigma_{\mu,MD}$, through the following procedures. [34, 32, 33] First, $\sigma_{\mu,MD}$ is calculated by the Monte Carlo evaluation of an integral based on trajectories that do not dissociate from the

MD/QCT calculations as follows,

$$\sigma_{\mu,MD} = \int \left(\frac{\hat{v}_{rel}^4}{4} \sin^2\chi + \frac{1}{3}(\Delta\hat{e}_{int})^2 - \frac{1}{2}(\Delta\hat{e}_{int})^2 \sin^2\chi \right) d\tau \tag{5.1}$$

where $\hat{v}_{rel}$ is the dimensionless relative collision velocity that is defined as $\sqrt{m_r/kT}v_{rel}$, $\Delta\hat{e}_{int}$ is the change in the dimensionless internal energy that is normalized by kT, and χ is the deflection angle that is defined as the change in the direction of the relative collision velocity vector between the collision pair in the beginning and at the end of the MD/QCT simulation. The internal energies and relative velocity,

$$v_{rel} = \sqrt{\frac{2E_c}{m_r}}, \tag{5.2}$$

are defined as initial conditions in the MD simulation and χ and $\Delta\hat{e}_{int}$ are obtained from the MD simulation data. The temperature, T, used in the normalization corresponds to the internal energy of the target sulfur dioxide molecule. The integration, $d\tau$, is performed over a range of initial orientations of the sulfur dioxide molecule and deflection angles. After $\sigma_{\mu,MD}$ is obtained, the equivalent variable hard sphere cross section, $\sigma_{VHS,MD}$, can be obtained as,

$$\sigma_{VHS,MD} = \frac{6\sigma_{\mu,MD}}{\hat{v}_{rel}^4} \tag{5.3}$$

Figure 5.2 compares the so computed MD/QCT viscosity cross sections with the VHS total cross sections used up to this point, that are based on the reference values given in Ref. [1]. The MD/QCT viscosity cross sections were obtained for the same set of internal energy values as discussed before. As shown in Fig. 5.2, the MD/QCT viscosity cross sections are generally larger than the earlier obtained VHS cross sections and can be seen to exhibit little dependence on the internal

energy, as expected. Note that we obtained values for the $E_{int} = 9.0 \times 10^{-19}$ J internal energy case as well, however, because the internal energy of the target is so close to the dissociation limit, it is difficult to separate the non-reacting from the reacting trajectories. Since the MD/QCT viscosity cross section is relatively independent of the internal energy we derive new MD/QCT based VHS parameters by curve fitting the MD results for $E_{int} = 4.0 \times 10^{-19}$ J to a VHS form. The new reaction probability table is then obtained by dividing the MD/QCT reaction cross section by the viscosity cross section at each collision energy. Comparison of Figs. 4.3 (RHS) and 5.3 shows that the applicable range of the MD/QCT chemistry model is now extended to higher collision energies than before and sufficiently high to cover the conditions of the two-dimensional simulations to be discussed in the next section.

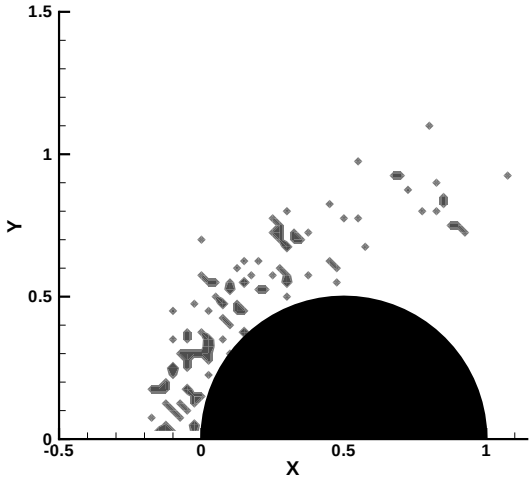

Figure 5.1. Locations in the counter flow where the reaction probability was found any time in the simulation to be greater than unity using the TCE model.

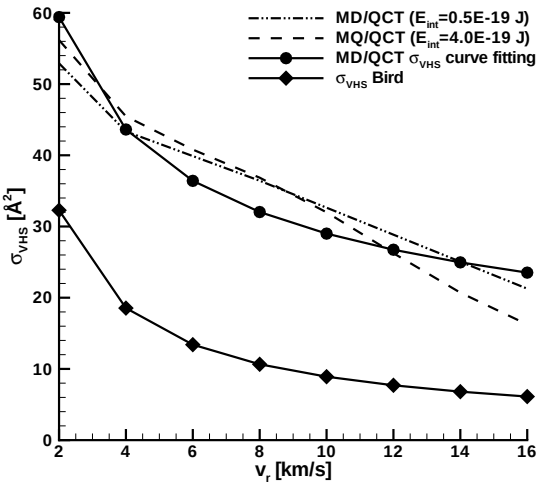

Figure 5.2. Comparison of MD/QCT viscosity cross sections with the VHS total cross sections based on the reference parameters of Bird.

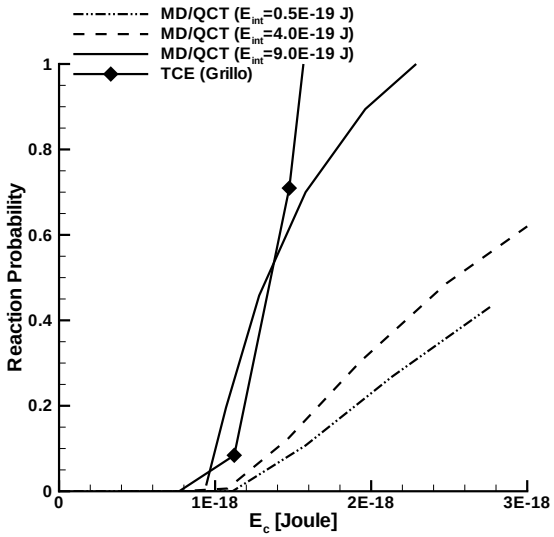

Figure 5.3. Reaction probabilities based on the MD/QCT reaction and viscosity cross sections.

Chapter 6

Evaluation of Two-dimensional DSMC Simulations Using MD/QCT Results

In this section, 2-D simulations relevant to planetary conditions were designed and performed to further evaluate the MD/QCT based collision and chemistry models implemented in DSMC. The 2-D axisymmetric test cases were set up to create a counter flow situation, in which the incoming O and the outgassing mixture of SO_2 and O from a sphere represents the flow coming from outer space and the volcanic plume from the surface of Io, respectively. Based on the work of Smyth *et al* [35], the initial number density ratio of the outgassing SO_2 to O was chosen to be 999 to 1, with a thermal temperature of 500 K. The speed of both the incoming and outgassing flows are set to be 10 km/s and the overall number density was 1.5×10^{18} molecule/m^3. The purpose of this flow configuration is to test the gas dynamics and chemistry in an approximate simulation of the highly complex bombarding plasma effect on the low atmospheric temperature of Io. [36] The incident plasma flow energizes a small portion of the low temperature atomic

oxygen, which in turn, reacts with the major Io atmospheric gas, SO_2.

Four different cases, summarized in Table 6.1, were considered in order to explore the sensitivity of the simulations to both the total and chemical reaction cross sections. The first case, the baseline, uses the VHS model based on the low temperature reference data given in Bird[1] and the TCE model based on the data of Grillo.[18] In the next DSMC simulation, case 2, the MD/QCT based viscosity cross section values are substituted for the VHS collisional cross section and at the same time the chemistry model is changed to use the MD/QCT based reaction probability table. Although our primary interest is to understand the influence of the chemistry models on the DSMC simulations, the SO reaction product will depend not only on the reaction cross section, but, on the total cross section as well. In other words, the number of collisions between O and SO_2 clearly depends on the collision cross section, and then, the number of reactions between these species will be affected by the chemistry model. The end result of the distribution of SO in the flowfield will be a mixture of both changes. Therefore, because we wanted to understand these two effects separately we ran two additional cases, designated in Table 6.1, as $1'$ and $2'$. These cases correspond to the unprimed cases except that there are *no* chemical reactions. In doing so, we can separate the effect of change in the collision model from those in the chemistry model on the gas dynamics of this plume-counter flow flowfield.

The comparisons of the two DSMC simulations at identical flow conditions with no reactions, cases $1'$ and $2'$, is shown first in Figs. 6.1 to 6.3. Since the O+SO_2 reaction is not modeled in the simulations, there are only O and SO_2 species in the flow field, undergoing collisions. Figures 6.1 and 6.2 show the predicted O and SO_2 in mole fractions and number densities, respectively, with case $1'$ on the top and case $2'$ on the bottom. As shown in the previous section, the MD/QCT

based viscosity cross sections are notably larger than the VHS cross sections at each relative velocity. Consequently, with fewer collisions between O and SO_2 in case $1'$, the O flow penetrates closer to the sphere, as shown in Fig. 6.1 (LHS). At the same time, because there are more collisions in case $2'$, the region where O is compressed, where the flow of O meets that of SO_2, exhibits a higher O number density, as shown in Fig. 6.1 (RHS). Similarly, Fig. 6.2 (LHS) shows that with fewer collisions between O and SO_2 in case $1'$, the outgassing SO_2 travels further away from the sphere, whereas, Fig. 6.2 (RHS) shows that with more collisions in case $2'$, the compressed region for SO_2 has higher number densities.

The flow structure can be further studied by examining the change in the streamlines of O and SO_2. One can examine changes in direction of the flow by selecting streamlines in each figure that start at the same location and comparing the locations of where those streamlines exit the computation domain. Figure 6.3 (LHS) shows that with fewer collisions in case $1'$, the change in direction of the incoming O flow is less than that in case $2'$, whereas Fig. 6.3 (RHS) shows that with more collisions in case $2'$, the change in direction of the out-gassing SO_2 flow is greater than that in case $1'$. The contour plots of mole fractions, number densities, and streamlines show that the total collisional cross section has a noticeable impact on the gas dynamics.

Now we turn to the effect of the chemistry model on the DSMC simulation results by comparing cases 1 and 2. Figure 6.4 shows a comparison of O, SO, and SO_2 number densities along the stagnation streamline and Fig. 6.5 shows the difference in the spatial distribution of the SO product mole fraction and number density for the two chemistry model cases. Note that comparison of DSMC simulations of cases 1 versus $1'$ and 2 versus $2'$ (not shown) revealed that there was no notable difference in the O and SO_2 both mole fractions or number densities.

This is an expected result because the reaction product SO can be seen in Fig. 6.4 to be a minor flow species and does not alter the main flow characteristics of O and SO_2. Figure 6.5 indicates that the DSMC simulation with the MD/QCT based VHS cross section (Eq. 5.3) and chemistry model (case 2, bottom) predicts a smaller region where SO is produced and a smaller amount of SO. The reaction region, the region where SO is produced, is similar to the compression region shown in case $2'$ discussed above. There are more collision between O and SO_2 in case 2, and consequently, less penetration of the outgassing SO_2 into the incoming O approaching the sphere (and visa versa) which results in a smaller reaction region. With regard to the amount of SO produced, Figs. 6.4 and 6.5 show that case 1 (TCE model) produces more products than case 2. This result is consistent with the fact that the reaction probabilities based on the TCE model using the data of Grillo[18] are higher than those obtained from the MD/QCT results (see Fig. 4.3). Moreover, this difference is noticeable because for the conditions in the DSMC 2-D simulations the target SO_2 has low internal energy.

Table 6.1. Two-dimensional DSMC Simulation Cases

Case	Description
1	VHS total cross section using low temperature reference data of Bird[1] and TCE model.
2	MD/QCT viscosity and chemical reaction cross sections.
$1'$	Same as Case 1, but, no chemical reactions.
$2'$	Same as Case 2, but, no chemical reactions.

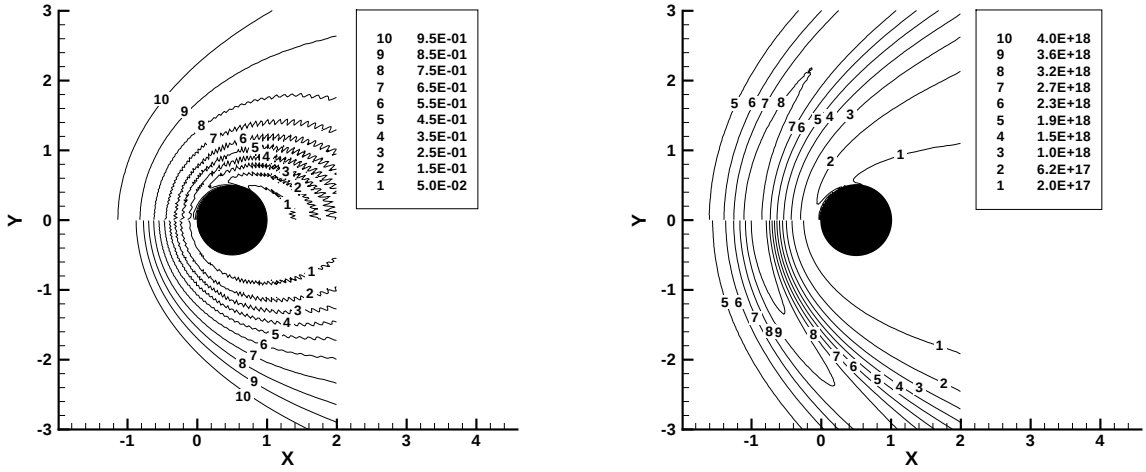

Figure 6.1. DSMC predictions, without reactions, of atomic oxygen spatial distributions, top - case $1'$ - the VHS model with Bird's values, bottom - case $2'$ - the VHS model based on MD/QCT viscosity cross sections. (LHS) Mole fraction of O and (RHS) Number density of O [/m^3]

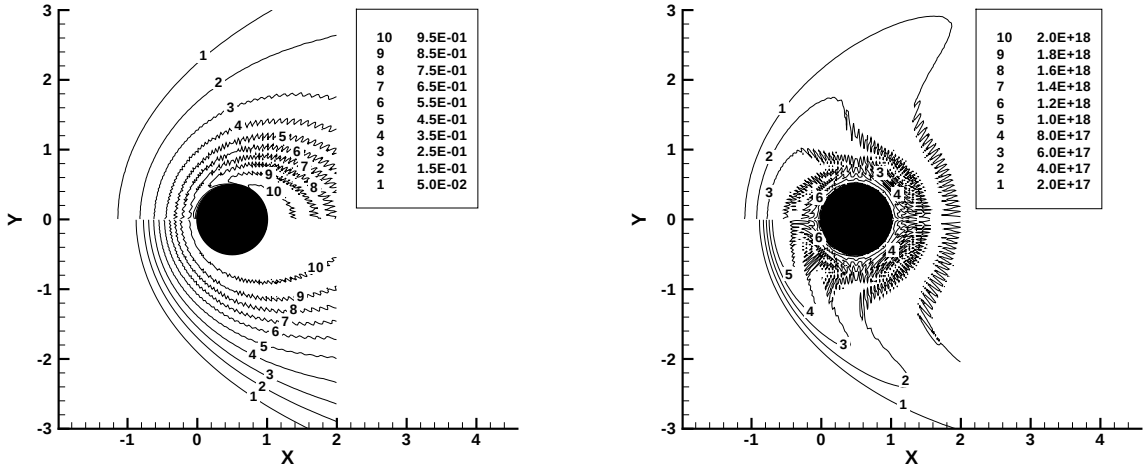

Figure 6.2. DSMC predictions, without reactions, of SO_2 spatial distributions, top - case $1'$ - the VHS model with Bird's values, bottom - case $2'$ - the VHS model based on MD/QCT viscosity cross sections. (LHS) Mole fraction of SO_2 and (RHS) Number Density of SO_2 [/m^3]

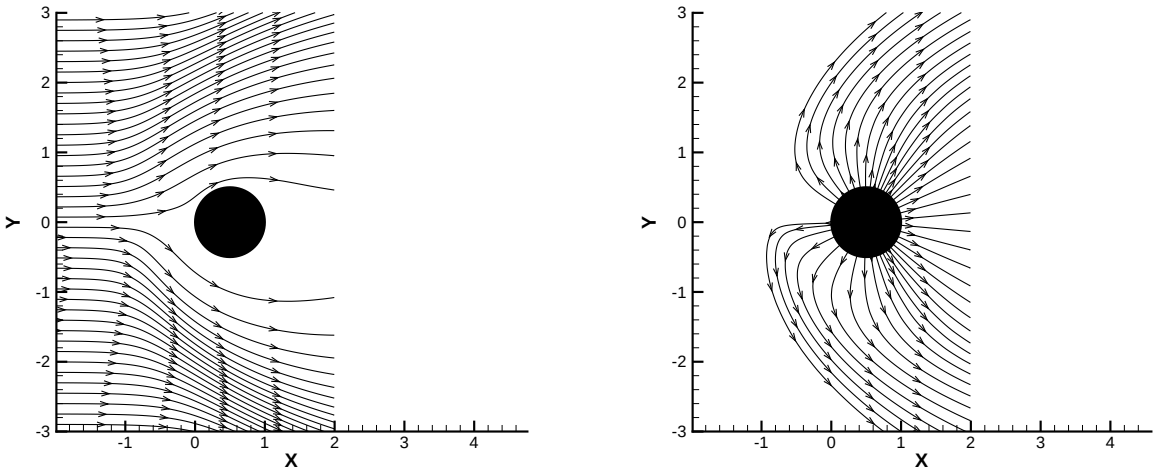

Figure 6.3. Streamlines of O and SO_2 obtained from the DSMC simulations without reactions, top - case $1'$ - the VHS model with Bird's values, bottom - case $2'$ - the VHS model based on MD/QCT viscosity cross sections. (LHS) O, (RHS) SO_2

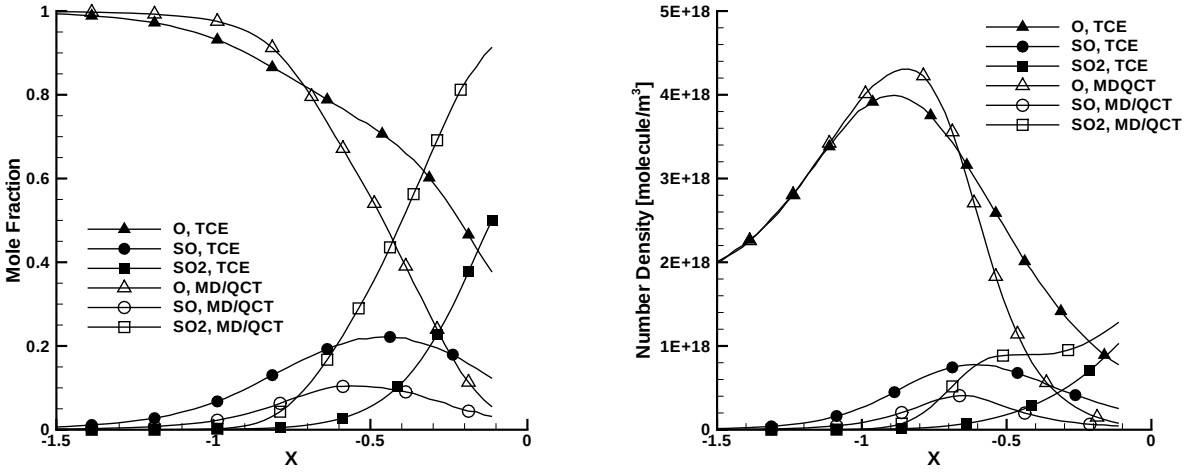

Figure 6.4. (LHS) Mole fraction and (RHS) number density components of SO along the stagnation line (Y = 0m) from the DSMC simulations, dashed - case 1 - Bird VHS model and Grillo TCE model, solid - case 2 - MD/QCT based VHS model and chemistry model. (LHS) Mole fraction and (RHS) Number density [/m^3]

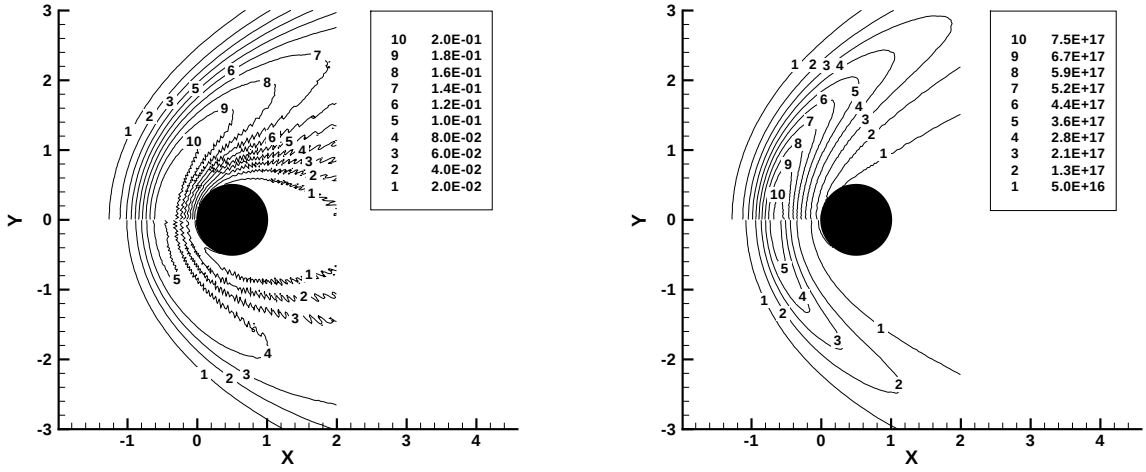

Figure 6.5. DSMC predictions of the SO spatial distributions , top - case 1 - Bird VHS model and Grillo TCE model, bottom - case 2 - MD/QCT based VHS model and chemistry model. (LHS) Mole fraction of SO and (RHS) Number density of SO [/m^3]

Chapter 7

Conclusions

Comparison of the MD/QCT rate constants and reaction probabilities with those derived from the TCE model shows that the former approach gives lower values. After validating the implementation of the chemistry models in DSMC through analyses of time dependent 0-D DSMC simulations, two approaches to utilize the MD/QCT results in the DSMC were examined. It was found that the curve-fitting of the reaction cross-sections method agrees fairly well with the tabulated reaction probability method, both of which are directly derived from the original MD/QCT results. Further investigations related to the sensitivity of the internal and total collisional energy ratio indicate that the use of tabulated reaction probabilities based on the MD/QCT results is capable of demonstrating the vibrational favoring feature of this dissociation reaction. The use of the TCE model resulted in similar changes in the DSMC simulation results, however, it was caused indirectly by the behavior of the temperature dependent internal degrees of freedom, ζ_{int}, in the model, rather than by the physical mechanism of vibrational favoring.

The atmospheric conditions of Io are challenging for DSMC simulations due to the high relative collisional velocity. Reaction probabilities based on TCE or MD/QCT reaction cross sections and the VHS total cross sections using the original

low temperature reference values of Bird were not guaranteed to be less than unity for all collisional required collisional energies. It was demonstrated that the baseline VHS collision cross section has a very different energy dependence than the MD/QCT based viscosity cross section and that use of the latter can extend the applicability of both collision model and chemistry model for DSMC for Io's conditions.

Finally, 2-D axisymmetric cases based on a simplified planetary condition of Io were performed. A two step analysis was used to fully evaluate the compound effects due to the change of collision and chemistry models by separating one from the other. In comparison with the DSMC simulation using conventional VHS and TCE models, the use of MD/QCT based VHS model leads to significant changes in the flow structure for the major species, O and SO_2, and the use of MD/QCT based reaction probabilities also lead to notable changes in terms of number density for the reaction product, SO.

Bibliography

[1] Bird, G. A. (1994) *Molecular Gas Dynamics and the Direct Simulation of Gas Flows*, chap. 2,6, Clarendon Press, Oxford, UK.

[2] Lopes, R. M. C. and J. R. Spencer (2007) *Io After Galileo: A New View of Jupiter's Volcanic Moon*, chap. 8, Praxis Publishing Ltd, Chichester, UK.

[3] Marchis, F., D. L. Mignant, F. Chaffeeb, A. Davies, S. Kwokb, R. Prangé, I. de Pater, P. Amicob, R. Campbell, T. Fuscoe, R. Goodrich, and A. Conradb (2005) "Keck AO survey of Io global volcanic activity between 2 and 5 μm," *Icarus*, **176**, pp. 96–122.

[4] Spencer, J. R., P. Sartoretti, G. E. Ballester, A. S. McEwen, J. T. Clarke, and M. A. McGrath (1997) "The Pele Plume (Io): Observations with the Hubble Space Telescope," *Geophys. Res. Lett.*, **24**, pp. 2471–2474.

[5] Moses, J. I., M. Y. Zolotov, and F. B., Jr. (2002) "Photochemistry of a Volcanically Driven Atmosphere on Io: Sulfur and Oxygen Species from a Pele-Type Eruption," *Icarus*, **156**, pp. 98–101.

[6] Moreno, M. A., G. Schubert, M. G. Kivelson, D. A. Paige, and J. Baumgardner (1991) "Io's volcanic and sublimation atmospheres," *Icarus*, **93**, pp. 63–81.

[7] Zhang, J., D. B. Goldstein, P. L. Varghese, N. E. Gimelshein, S. F. Gimelshein, and D. A. Levin (2003) "Simulation of Gas Dynamics and Radiation in Volcanic Plumes on Io," *Icarus*, **163**, pp. 182–197.

[8] Austin, J. V. and D. B. Goldstein (1995) "Direct numerical simulation of low density atmospheric flow on Io," in *Molecular Physics and Hypersonic Flows*, Kluwer Academic Publishers, Dordrechit, The Netherlands.

[9] ——— (1998) "Simulation of Supersonic Rarefied Atmospheric Flows on Io," in *Rarefied Gas Dynamics: Proceedings of the 21st International Symposium on Rarefied Gas Dynamics*, vol. 2, Cepadues-Editions, Toulouse, France.

[10] Zhang, J., D. B. Goldstein, P. L. Varghese, N. E. Gimelshein, S. F. Gimelshein, D. A. Levin, and L. M. Trafton (2003) "DSMC Modeling of Gas Dynamics, Radiation and Particulates in Ionian Volcanic Jets," in *Proceedings of 23rd International Symposium on Rarefied Gas Dynamics*, vol. 663, AIP, New York.

[11] Zhang, J., K. Miki, D. B. Goldstein, P. L. Varghese, and L. M. Trafton (2003) "Modeling of Radiation Above Io's Surface from Pele-type Volcanic Plumes and Underground form the Conduit Wall," *Lunar and Planet. Sci. XXXIV*, abstract no. 2123.

[12] Zhang, J., D. B. Goldstein, P. L. Varghese, L. M. Trafton, K. Miki, and C. Moore (2004) "Numerical Modeling of Ionian Volcanic Plumes with Entrained Particulates," *Icarus*, **172**, pp. 479–502.

[13] Moghe, N. V. (2007) *Molecular Dynamics Simulations of Collisionally Induced Dissociation of Sulfur Dioxide, an Atmospheric Species of Io*, Master's thesis, Department of Aerospace Engineering, The Pennsylvania State University.

[14] Deng, H., C. Moore, D. Levin, and D. Goldstein (2011) "Analysis of SO_2+O Chemistry Models for Simulations of the Atmosphere on Io," in *Proceedings of the 27th International Symposium on Rarefied Gas Dynamics - in press*, American Institute of Physics, New York.

[15] Bose, D. and G. V. Candler (1996) "Thermal Rate Constants of the N_2+O $\rightarrow$ NO+N Reaction Using *Ab Initio* $^3A''$ and $^3A'$ Potential Energy Surfaces," *Journal of Chemical Physics*, **104**(8), pp. 2825–2833.

[16] Ozawa, T., D. Fedosov, D. A. Levin, and S. F. Gimelshein (2005) "Quasi-Classical Trajectory Modeling of OH Production in Direct Simulation Monte Carlo," *Journal of Thermophysics and Heat Transfer*, **19**(2), pp. 235–244.

[17] Levin, D. A. and S. F. Gimelshein (2000) "Modeling of OH Vibrational Distributions Using Molecular Dynamics with the Direct Simulation Monte Carlo Method," *AIAA Paper*.

[18] Grillo, A., R. Reed, and M. W. Slack (1979) "Infrared Measurements of Sulfur Dioxide Thermal Decomposition Rate in Shock Waves," *J. Chem. Phys.*, **70**(4), pp. 1634–1636.

[19] Abramowitz, M. and I. A. Stegun (1970) *Handbook of Mathematical Functions, with Formulas, Graphs, and Mathematical Tables*, Dover Publications, New York.

[20] Wilson, E. B., J. C. Decius, and P. C. Cross (1955) *Molecular Vibrations*, McGraw Hill, New York.

[21] Noid, D. W., M. L. Koszykowshi, and R. A. J. Marcus (1977) "A Spectral Analysis Method of Obtaining Molecular Spectra from Classic Trajectories," **67**(2).

[22] Redmon, M. J., R. J. Bartlett, B. C. Garett, and G. D. Purvis (1981) *Potential Energy Surface and Dynamics Calculations*, New York.

[23] Astholz, D., K. Glanser, and J. Troe (1978) "UV Absorption Study of the Thermal Decomposition of SO, SO_2, and SO_3," in *Proceedings of the 11th International Symposium on Shock Tubes and Shock Waves*, University of Washington, Seattle.

[24] Olschewski, H. A., J. Troe, and H. G. Wagner (1965) "Der unimolekulare Zerfall von SO2," *Z. Phys. Chem.*, **44**, pp. 173–183.

[25] Kee, R. J., F. M. Rupley, and J. A. Miller (1987) *The Chemkin Thermodynamic Data Base*, *Tech. Rep. SAND-87-8215*, Sandia National Labs.

[26] ——— (1989) *Chemkin-II: A Fortran Chemical Kinetics Package for the Analysis of Gas-Phase Chemical Kinetics*, *Tech. Rep. SAND-89-8009*, Sandia National Labs.

[27] Ivanov, M. S., G. N. Markelov, and S. F. Gimelshein (1998) "Statistical Simulation of Reactive Rarefied Flows: Numerical Approach and Applications," in *AIAA Paper*, AIAA/ASME Joint Thermophysics and Heat Transfer Conference, 7th, pp. 1998–2669.

[28] Ivanov, M. S. and S. V. Rogasinsky (1988) "Analysis of the Numerical Techniques of the Direct Simulation Monte Carlo Method in the Rarefied Gas Dynamics," *Soviet Journal of Numerical Analysis and Mathematical Modeling*, **3**(6), pp. 453–465.

[29] Borgnakke, C. and P. S. Larsen (1975) "Statistical Collision Model for Monte Carlo Simulation of Polyatomic Gas Mixture," *Journal of Computational Physics*, **18**(4), pp. 405–420.

[30] Millikan, R. C. and D. R. White (1963) "Systematics of vibrational relaxation," *J. Chem. Phys.*, **39**, p. 3209.

[31] Parker, J. G. (1959) "Rotational and vibrational relaxation in diatomic gases," *Phys. Fluids*, **2**, p. 449.

[32] Ozawa, T., D. A. Levin, and I. J. Wysong (2007) "Chemical Reaction Modeling for Hypervelocity Collisions between O and HCl," *Physics of Fluids*, **19**(5), p. 14.

[33] Tokumasu, T. and Y. Mastumoto (1999) "Dynamic Molecular Collision (DMC) Model for Rarefied Gas Flow Simulations by the DSMC Method," *Physics of Fluids*, **11**.

[34] Lordi, J. A. and R. E. Mates (1970) "Rotational Relaxation in Nonpolar Diatomic Gases," *Physics of Fluids*, **13**.

[35] Smyth, H. W. and C. M. Wong (2004) "Impact of Electron Chemistry on the Structure and Composition of Io's Atmosphere," *Icarus*, **171**, p. 176.

[36] Moore, C. H., D. B. Goldstein, P. L. Varghese, L. M. Trafton, and B. Stewart (2009) "1-D DSMC simulation of Io's atmospheric collapse and reformation during and after eclipse," *Icarus*, doi:10.1016/j.icarus.2009.01.006.